

Effects of local nonequilibrium in rapid eutectic solidification—Part 1: Statement of the problem and general solution

Junfeng Xu^{1,2}  | Peter K. Galenko^{1,3} 

¹Physikalisch-Astronomische Fakultät, Friedrich-Schiller-Universität Jena, Jena, Germany

²School of Materials and Chemical Engineering, Xi'an Technological University, Xi'an, China

³Laboratory of Multi-scale Mathematical Modeling, Department of Theoretical and Mathematical Physics, Ural Federal University, Ekaterinburg, Russia

Correspondence

Peter K. Galenko, Physikalisch-Astronomische Fakultät, Friedrich-Schiller-Universität Jena, Jena 07743, Germany.

Email: peter.galenko@uni-jena.de

Funding information

Natural Science Foundation of Shaanxi Provincial Department of Education, Grant/Award Number: 18JS050; Key Science and Technology Program of Shaanxi Province, Grant/Award Number: 2016KJXX-87; German Space Center Space Management, Grant/Award Number: 50WM1941

Numerous experimental data on the rapid solidification of eutectic systems exhibit the formation of metastable solid phases with the initial (nominal) chemical composition. This fact is explained by suppression of eutectic decomposition due to diffusionless (chemically partitionless) solidification beginning at a high but a finite growth velocity of crystals. A model considering the diffusionless growth is developed in the present work to analyze the atomic diffusion ahead of lamellar eutectic couples growing into supercooled liquid. A general solution of the model is presented from which two regimes are followed. The first presents a diffusion-limited regime with the existence of eutectic decomposition if the solid–liquid interface velocity is smaller than the characteristic diffusion speed in the bulk liquid. The second shows suppression of eutectic decomposition under diffusionless transformation from liquid to one-phase solid if the solid–liquid interface velocity overcomes characteristic diffusion speed in the bulk liquid.

KEY WORDS

diffusion, eutectic growth, interface, model, solute

MSC CLASSIFICATION

80A22; 82C26

1 | INTRODUCTION

Eutectic transformation presents the decomposition of one phase to the other ones resulting in the formation of mechanical mixture of solid phases. The transformation has many evidences that the eutectic microstructure is affected by undercooling and growth velocity in the case of solidification from undercooled liquid and by thermal gradient in the case of unidirectional solidification.¹ At low undercoolings or small growth velocities, the eutectic structure has lamellar, rod, or irregular morphology,² while at high undercooling or large growth velocity, anomalous eutectic

[Correction added on 23 October, after first online publication: Projekt Deal funding statement has been added.]

This is an open access article under the terms of the Creative Commons Attribution-NonCommercial License, which permits use, distribution and reproduction in any medium, provided the original work is properly cited and is not used for commercial purposes.

© 2020 The Authors. Mathematical Methods in the Applied Sciences published by John Wiley & Sons Ltd

will appear instead of regular or irregular eutectic patterns.³ There are many experimental works, especially for Ni–Sn,³ Co–Si, Ni–Si,⁴ Fe–B, Co–B, Ni–B,⁵ Al₂O₃–Er₃Al₅O₁₂ alloys,⁶ in which such changes in morphology were found.

If the growth velocity is provided by deep undercooling or ultrafast cooling rates, the metastable single phase of crystals or glass can be formed. For example, using the injection of a liquid droplet into a quenching bath, Duwez et al. obtained crystalline microstructure with metastable solid solution of the single phase instead of expected eutectic pattern in Ag–Cu alloys.⁷ Giessen et al. found that the eutectic transformation in Y–Cu alloy should be suppressed, and a metastable solid solution can be formed by using the “splat cooling” technique.⁸ In addition to this, Miroshnichenko found homogeneous supersaturated solid solutions of the initial composition in Al–Mg eutectic alloy after quenching from the melts at rates of 10⁵–10⁶ K s⁻¹.⁹ The same outcome has been also reported by Jacobson¹⁰ in a series of experiments on films from Ag–Cu alloys processed by melt-spinning. In addition to the observations of diffusionless solidification of eutectic (or near eutectic) melts, one can also find some characteristic types of crystal microstructures indicating the existence of chemically partitionless crystal growth. For example, Gusakova et al.¹¹ studied the effect of the cooling rate on the microstructure and showed that at cooling rates of about 10⁵ K s⁻¹, the eutectic reaction of Sn–Bi alloys is suppressed, and grains of a supersaturated solid solution of Bi in Sn are formed by partitionless solidification.

Jackson and Hunt (JH) gave the first model for diffusion-limited growth of lamellar and rod eutectics as the growth of coupled α and β phases.¹² Datye and Langer performed a stability analysis for the JH model of a directionally solidifying, thin-film, lamellar eutectic the stability of thin lamellar eutectic growth.¹³ Trivedi et al., relaxing the assumptions of small Peclet numbers, used cigar-shaped phase diagram and equal-distribution-coefficients phase diagram and extended the JH model to the eutectic growth under rapid solidification conditions (Trivedi–Magnin–Kurz [TMK] model).¹⁴ Taking the interface solute trapping into account, Kurz et al. analyzed the failure of local equilibrium at the solid–liquid interface within the framework of the JH and TMK models and found that the chemical distribution coefficient k is no longer constant but depends on the eutectic growth velocity.¹⁵ Based on the previous models, Ludwig and Zheng et al. obtained the ΔT – V – λ relationship for arbitrary binary eutectic phase diagrams (including $k_\alpha \neq k_\beta$) and arbitrary Peclet number together with the general scaling law for eutectic growth.^{16,17} Their calculation procedure, however, exhibited difficulties in obtaining the reliable results due to iterative method and slow convergence to the final value. Li et al. neglected the solute trapping but incorporated the kinetic and thermal undercoolings into the eutectic growth to analyze solidification in bulk undercooled melt (Li–Zhou [LZ] model).¹⁸ Then Wei et al. developed the LZ model to analyze the anomalous eutectic formation in alloy melt.¹⁹

Although the regular eutectics form at small undercooling and anomalous patterns appear at deeply undercooled eutectic systems that can be described by one of the latest models,^{12–19} the results for the diffusionless microstructure cannot be predicted by these models. The diffusionless theory in eutectic systems²⁰ gives the solution for concentration profiles and indicates that the predicted transition from eutectic couples to chemically partitionless crystal growth exists consistently with experimental findings qualitatively. To give predictions comparable with experimental data quantitatively, the model should predict lamellar spacing and growth velocity as a function of cooling rate or undercooling. Therefore, in this study, we shall develop a complete model building upon the theory²⁰ to predict the transition to diffusionless solidification, and we use the treatment of LZ model¹⁸ to write an undercooling balance as a function of the lamellar spacing and growth velocity. The resulting eutectic model will include the final speed V_D for solute diffusion in the bulk liquid that will allow us to predict the complete solute trapping and diffusionless solidification at the finite interface velocity.²¹

2 | MODEL EQUATIONS

2.1 | The model statement

Consider solidification of a binary system consisting of the atoms A and B and having the eutectic point with equilibrium temperature T_E and concentration C_E , as shown in Figure 1A. ΔC_α and ΔC_β are the concentration differences between phases α , β , and eutectic point (T_E , C_E), respectively.

Assume that undercooling ΔT below eutectic point in the liquid provides a motion of the interface with the velocity V comparable with the solute diffusion speed $V_D = \sqrt{D/\tau_D}$ in bulk liquid,²⁰ where D is the diffusion coefficient and τ_D is the time for relaxation of solute diffusion flux to its steady-state value. We neglect the diffusion in α and β phases, which have the form of the lamellar eutectic microstructure. In steady-state regime, the two dimensional diffusion equation for the concentration C of B atoms in liquid given by^{20,21}

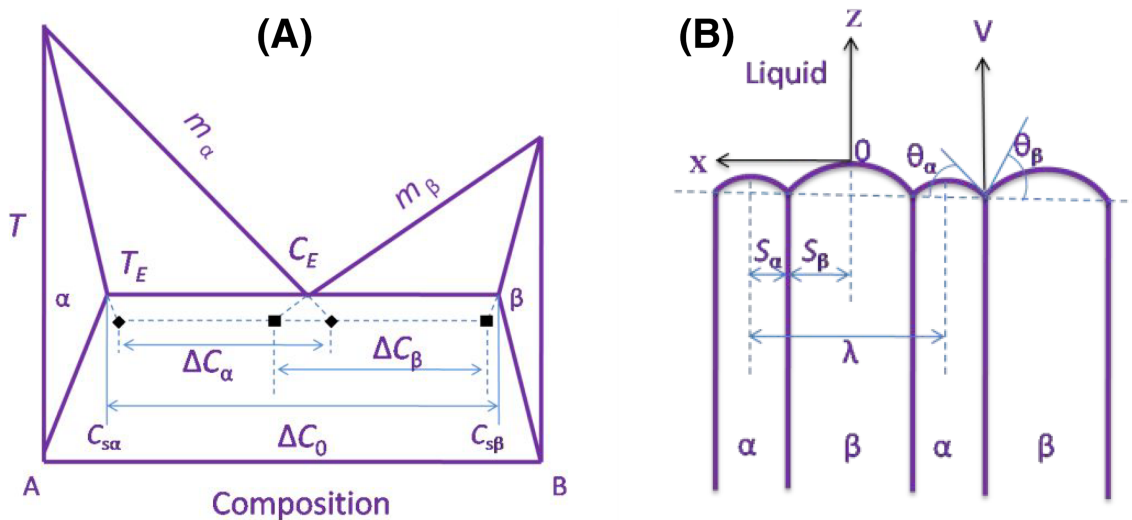


FIGURE 1 Scheme of eutectic phase diagram (A) and the growing lamellar eutectic structure (B) [Colour figure can be viewed at wileyonlinelibrary.com]

$$\frac{\partial^2 C}{\partial x^2} + \left(1 - \frac{V^2}{V_D^2}\right) \frac{\partial^2 C}{\partial z^2} + \frac{V \partial C}{D \partial z} = 0 \quad (1)$$

which is valid for concentration $C(x,y)$ in the spatial reference frame (x,y) moving at a constant velocity V at the interface $z=0$. For eutectic transformation, the boundary conditions are²⁰

$$\begin{aligned} & \text{-- periodicity : } C(x+\lambda) = C(x), \text{ here } \lambda = 2(S_\alpha + S_\beta) \\ & \text{-- symmetry : } \partial C / \partial z = 0 \text{ for } x = 0 \text{ and } x = \lambda/2 = S_\alpha + S_\beta \\ & \text{-- far-field : } C = C_\infty \text{ for } z \rightarrow \infty \end{aligned} \quad (2)$$

where S_α and S_β represent the half of interlamellar spacing for each phase such that $\lambda = 2(S_\alpha + S_\beta)$ is the lamellar spacing (see Figure 1B) and C_∞ is the concentration in the liquid far from the interface.

For Equations 1 and 2, an analytical solution of the problem of lamellar eutectic pattern under local nonequilibrium conditions in the solute diffusion field has been obtained by Galenko and Herlach.²⁰ The general solution for growth of periodic lamellas is described as,²⁰

$$C = C_\infty + B_0 \exp \left[-\frac{Vz}{D(1-V^2/V_D^2)} \right] + \sum_{n=1}^{\infty} B_n \cos(b_n x) \exp(-\omega_n z), \quad V < V_D \quad (3a)$$

$$C = C_\infty, \quad V \geq V_D \quad (3b)$$

$$\omega_n = \frac{V}{2D(1-V^2/V_D^2)} + \left[\left(\frac{V}{2D(1-V^2/V_D^2)} \right)^2 + b_n^2 \right]^{1/2} \quad (3c)$$

$$b_n = n\pi / (S_\alpha + S_\beta) \quad (3d)$$

where B_0 and B_n are the Fourier coefficients and n belongs to a set of integer values. To calculate B_0 and B_n , we use the boundary conditions from mass conservations^{18,20}:

-solute balance at the interface for α phase ($0 \leq x < S_\alpha$)

$$-D\left(1 - \frac{V^2}{V_D^2}\right)\left(\frac{\partial C}{\partial z}\right)_{z=0} = VC(x, 0)(1 - k_\alpha) = V(C_{l\alpha} - C_{s\alpha}) \quad (4a)$$

-solute balance at the interface for β phase ($S_\alpha \leq x < S_\alpha + S_\beta$)

$$-D\left(1 - \frac{V^2}{V_D^2}\right)\left(\frac{\partial C}{\partial z}\right)_{z=0} = -V[1 - C(x, 0)](1 - k_\beta) = -V(C_{l\beta} - C_{s\beta}) \quad (4b)$$

Here, k_α and k_β are the velocity-dependent solute partitioning functions for α phase and β phase, respectively, at the interface; $C_{l\alpha}$ and $C_{l\beta}$ are the concentrations on α phase and β phase in the liquid, respectively; $C_{s\alpha}$ and $C_{s\beta}$ are the concentrations on α phase and β phase in the solid (see Figure 1A).

The following features of solutions (3) and (4) can be outlined. *First*, one can note that the only diffusion equation gives two principally different regimes. One of them occurs with $V < V_D$ leading to inhomogeneous composition in both longitudinal direction (along the z -axis) and transverse direction (along the x -axis) of solute distribution around the interface. In this regime, eutectic decomposition is determined by the atomic diffusion because the eutectic lamellar couples can grow through the inhomogeneous solute field. Another regime proceeds with $V \geq V_D$ leading to homogeneous composition of the initial (nominal) concentration in both spatial directions. Due to chemical homogeneity around the interface, the growth of eutectic couples is not possible. Such high-rate regime is usually called as “chemically partitionless” or merely “diffusionless” regime of solidification. *Second*, as distinct from the classical Jackson-Hunt solution,¹² spatial frequency includes the term with $V/2D$ in addition to the term b_n , determined by Equation 3d. In this description, the term $V/[2D(1 - V^2/V_D^2)]$ in Equation 3a increases at $V \rightarrow V_D$ and, evidently, becomes a significant function of the velocity V , especially at $V \approx V_D$. *Third*, Equation (3) is transformed to the known solution of the TMK model¹⁴ for local equilibrium limit $V_D \rightarrow \infty$ in the diffusion field. *Fourth*, when periodicity is lacking, that is, $b_n = 0$, solution (3) describes the concentration profile of single-phase solidification at a finite diffusion speed V_D .²⁰

If $V < V_D$, the lamellar eutectic structure does not form; therefore, we firstly consider the case of $V < V_D$. After this, a discussion for the high rate regime $V \geq V_D$ will be provided.

2.2 | Fourier coefficients

The solution for concentration gradient ahead of the eutectic interface is found by differentiating Equation 3a with respect to z . This yields the z -component of the concentration gradient, which periodically varies in the x -direction and exponentially damped in the z -direction:

$$\left.\frac{\partial C}{\partial z}\right|_{z=0} = -\frac{V}{D(1 - V^2/V_D^2)}B_0 - \sum_{n=1}^{\infty} B_n \left(\frac{n\pi}{S_\alpha + S_\beta}\right) \cos\left(\frac{n\pi x}{S_\alpha + S_\beta}\right) \quad (5)$$

Substituting Equation 5 into Equation 4a, one can obtain for α phase ($0 \leq x < S_\alpha$).

$$\begin{aligned} \int_0^{S_\alpha} \frac{\partial C}{\partial z} dz \Big|_{z=0} &= -B_0 S_\alpha \frac{V}{D1 - V^2/V_D^2} - \sum_{n=1}^{\infty} B_n \frac{n\pi}{S_\alpha + S_\beta} \sin\frac{n\pi S_\alpha}{S_\alpha + S_\beta} \\ &= -\frac{V}{D1 - V^2/V_D^2} Cx, 01 - k_\alpha S_\alpha \end{aligned} \quad (6a)$$

Substituting Equation 5 into Equation 4b, one finds for β phase ($S_\alpha \leq x < S_\alpha + S_\beta$).

$$\begin{aligned} \int_{S_\alpha}^{S_\alpha + S_\beta} \left(\frac{\partial C}{\partial z} \right)_{z=0} dx &= -B_0 S_\beta \left(\frac{V}{D(1-V^2/V_D^2)} \right) + \sum_{n=1}^{\infty} B_n \left(\frac{n\pi}{S_\alpha + S_\beta} \right) \sin \left(\frac{n\pi S_\alpha}{S_\alpha + S_\beta} \right) \\ &= \frac{V}{D(1-V^2/V_D^2)} [1 - C(x, 0)] (1 - k_\beta) S_\beta \end{aligned} \quad (6b)$$

To obtain the solution for B_0 and B_n , we shall follow the treatments of TMK model with the two special types of phase diagrams. The first case is related to cigar-shaped phase diagram (Figure 2A), and the second case is related to the equal distribution coefficients (Figure 2B).

2.2.1 | Case I: Cigar-shaped phase diagram

For this type of phase diagram, the solidus and the liquidus lines are parallel below the eutectic temperature. In this case (Figure 2A), for any undercooling, it can be obtained $C_{l\alpha} - C_{s\alpha} = \Delta C_\alpha = \text{const}$ and $C_{l\beta} - C_{s\beta} = \Delta C_\beta = \text{const}$.¹⁴ The distribution coefficient k varies from that at eutectic temperature to unity as the undercooling is increased. In general, if the two eutectic phases have a higher solubility, or the solidus line is bent upward and the liquidus line is bent downward, which will lead to parallel lines below eutectic temperature, the equations of Case I can be used, such as Fe-C and Al-Cu phase diagrams.²² The coefficient B_0 can thus be worked out by adding both sides of Equations 6a and 6b:

$$B_0 = \frac{\Delta C_\alpha S_\alpha - \Delta C_\beta S_\beta}{S_\alpha + S_\beta} \quad (7a)$$

For solution of the coefficients B_n , one can refer to the integral series^{14,23} that leads to the following:

$$B_n = \frac{2}{(n\pi)^2} \frac{n\pi V}{\omega_n D} \frac{\Delta C_0}{(1-V^2/V_D^2)} \sin(n\pi f_\alpha) \quad (7b)$$

where $\Delta C_0 = \Delta C_\alpha + \Delta C_\beta$, and $f_\alpha = S_\alpha/(S_\alpha + S_\beta)$.

2.2.2 | Case II: Equal distribution coefficients for the two phases

For this case (Figure 2B), k is an arbitrary constant, but $k_\alpha = k_\beta = k$. There is $\Delta C_\alpha + \Delta C_\beta = \Delta C_0 = 1 - k$. One of the characters is, $C_{s\alpha}$ increases with C_E and $C_{s\beta}$ increases with $(1 - C_E)$. Generally, if the solid solubility of the two eutectic phases is small, the equations of Case II can be used, such as Fe-B and Co-B phase diagrams.²² Using Equations 6a and 6b, one arrives at,

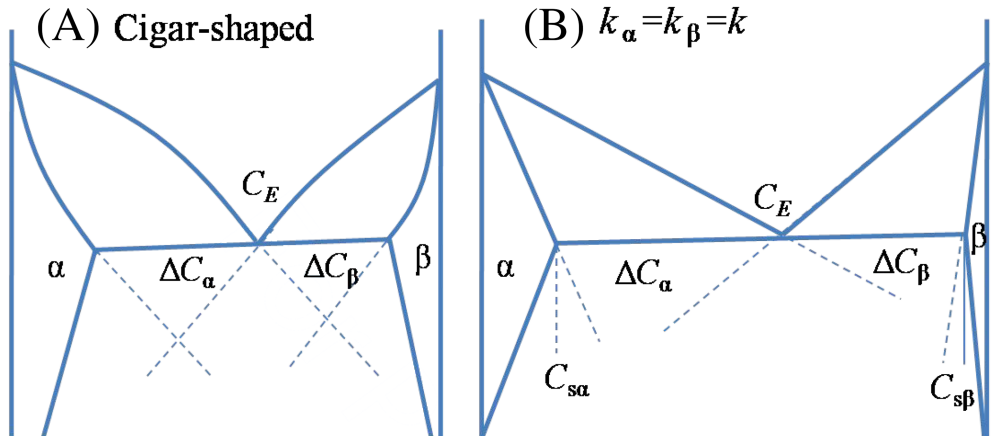


FIGURE 2 Two special types of phase diagram in TMK model: (A) Case II; (B) Case II [Colour figure can be viewed at wileyonlinelibrary.com]

$$B_0 = \frac{(1-k)C_\infty S_\alpha - (1-C_\infty)S_\beta}{k(S_\alpha + S_\beta)} \quad (8a)$$

$$B_n = \frac{2(S_\alpha + S_\beta)V}{(n\pi)^2} \frac{p_n(1-k)\sin(n\pi f_\alpha)}{D \sqrt{1 + [p_n(1-V^2/V_D^2)]^2} - 1 + 2k} \quad (8b)$$

where $p_n = 2n\pi/Pe$ with the eutectic Peclet number $Pe = V\lambda/(2D)$.

2.3 | Interfacial chemical composition ($V < V_D$)

For the undercooling calculation, the interfacial average composition in liquid is obtained from the LZ treatment.¹⁸ Using Equation 3a, the results are as follows:

-in front of the α phase

$$\bar{C}_\alpha = C_\infty + B_0 + \frac{1}{S_\alpha} \int_0^{S_\alpha} \sum_{n=1}^{\infty} B_n \cos(b_n x) dx = C_\infty + B_0 + \frac{2(S_\alpha + S_\beta)^2 V}{S_\alpha D} (1-k) P \quad (9a)$$

-in front of the β phase

$$\bar{C}_\beta = C_\infty + B_0 - \frac{1}{S_\beta} \int_0^{S_\beta} \sum_{n=1}^{\infty} B_n \cos(b_n x) dx = C_\infty + B_0 - \frac{2(S_\alpha + S_\beta)^2 V}{S_\alpha D} (1-k) P \quad (9b)$$

The function P in Equation (9) is obtained accordingly the above two cases of the phase diagram as follows:

Case I. Cigar-shaped phase diagram

$$P = \sum_{n=1}^{\infty} \frac{\sin^2(n\pi f_\alpha)}{(n\pi)^3} \frac{p_n}{\sqrt{1 + [p_n(1-V^2/V_D^2)]^2} + 1} \quad (10a)$$

$$P + \lambda \frac{\partial P}{\partial \lambda} = \sum_{n=1}^{\infty} \frac{\sin^2(n\pi f_\alpha)}{(n\pi)^3} \left(\frac{p_n(1-V^2/V_D^2)}{\sqrt{1 + [p_n(1-V^2/V_D^2)]^2} + 1} \right)^2 \frac{p_n}{\sqrt{1 + [p_n(1-V^2/V_D^2)]^2}} \quad (10b)$$

Case II. The diagram with equal distribution coefficients

$$P = \sum_{n=1}^{\infty} \frac{\sin^2(n\pi f_\alpha)}{(n\pi)^3} \frac{p_n}{\sqrt{1 + [p_n(1-V^2/V_D^2)]^2} - 1 + 2k} \quad (11a)$$

$$P + \lambda \frac{\partial P}{\partial \lambda} = \sum_{n=1}^{\infty} \frac{\sin^2(n\pi f_\alpha)}{(n\pi)^3} \left(\frac{p_n(1-V^2/V_D^2)}{\sqrt{1 + [p_n(1-V^2/V_D^2)]^2} - 1 + 2k} \right)^2 \frac{p_n}{\sqrt{1 + [p_n(1-V^2/V_D^2)]^2}} \quad (11b)$$

Together with Equations (7) and (8), the solute concentration at the interface is completely defined by expressions (9)–(11). Note that if the solidification range interval becomes narrower, $k \rightarrow 1$, Case II transforms to the Case I.

2.4 | Interfacial undercooling ($V < V_D$)

The undercooling at interface “liquid-eutectic pattern” consists of four terms: constitutional undercooling ΔT_c , the curvature undercooling (due to Gibbs–Thomson effect) ΔT_r , the kinetic undercooling ΔT_k , and the thermal undercooling ΔT_t . The sum of the first three terms comprises the so-called interfacial undercooling. For each phase, it is given by.¹⁸

$$\Delta T_I = T_E - T_I = \Delta T_c + \Delta T_r + \Delta T_k = m_i^v(C_E - C) + \Gamma_i \frac{\sin\theta_i}{S_i} + \frac{V}{\mu_i} \quad (12)$$

where T_E is the equilibrium eutectic temperature, m_i^v is the velocity-dependent liquidus line slope, Γ_i is the Gibbs–Thomson coefficient (ratio of the surface energy to melting entropy per unit volume), θ_i is the contact angle at the triple point junction (see Figure 1B in which “ $i = \alpha$ or β ”), S_i is the half the width of the lamellar, and μ_i is the effective kinetic coefficient for growth of each eutectic phase. Following the procedure described by the TMK model,¹⁴ the average undercooling at the interface for lamellar eutectic pattern is obtained by inserting average values for concentration (\bar{C}_α and \bar{C}_β) and curvatures ($\sin\theta_\alpha/S_\alpha$ and $\sin\theta_\beta/S_\beta$) of the α phase and β phase, respectively. From Equation 12, the undercoolings at the front of α phase and β phase are described by the following.¹⁸

$$\Delta T_\alpha = m_\alpha^v(\bar{C}_\alpha - C_E) + \Gamma_\alpha \frac{\sin\theta_\alpha}{S_\alpha} + \frac{V}{\mu_\alpha} \quad (13a)$$

$$\Delta T_\beta = m_\beta^v(C_E - \bar{C}_\beta) + \Gamma_\beta \frac{\sin\theta_\beta}{S_\beta} + \frac{V}{\mu_\beta} \quad (13b)$$

The solid–liquid interfaces of regular lamellar eutectics are usually assumed to be isothermal. Therefore, one can accept the equality: $\Delta T_\alpha = \Delta T_\beta = \Delta T_I$. To eliminate the terms involving C_E , we combine Equation (9) with Equation (13) and find the interfacial undercooling as follows.¹⁸

$$\Delta T_I = m^v \left[\left(Q_0^L \lambda + \frac{1}{\mu} \right) V + \frac{a^L}{\lambda} \right] \quad (14)$$

where

$$Q_0^L = \frac{1 - kP}{f_\alpha f_\beta D} \quad (15)$$

$$a^L = 2 \left(\frac{\Gamma_\alpha \sin\theta_\alpha}{m_\alpha^v f_\alpha} + \frac{\Gamma_\beta \sin\theta_\beta}{m_\beta^v f_\beta} \right) \quad (16)$$

$$m^v = \frac{m_\alpha^v m_\beta^v}{m_\alpha^v + m_\beta^v} \quad (17)$$

$$\mu = \frac{m_\alpha^v m_\beta^v \mu_\alpha \mu_\beta}{m_\alpha^v \mu_\alpha + m_\beta^v \mu_\beta} \quad (18)$$

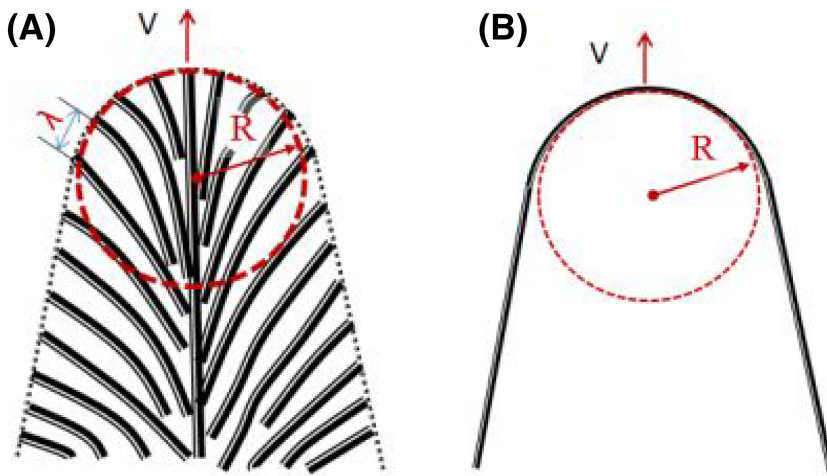


FIGURE 3 Scheme of eutectic tip shown as dendritic surface: (A) diffusion-limited growth of eutectic dendrite at $\lambda \ll R$, $V < V_D$; (B) diffusionless growth of dendrite having eutectic composition but with suppressing eutectic decomposition at $V \geq V_D$ [Colour figure can be viewed at wileyonlinelibrary.com]

Consider the macro-interface as the dendritic surface with the dendrite tip radius R much larger than interlamellar spacing, $\lambda \ll R$ (Figure 3A), following the previous treatments, the thermal undercooling can be described as¹⁸

$$\Delta T_t = \frac{\Delta H}{C_p} Iv(P_t) \quad (19)$$

where $\Delta H = f_\alpha \Delta H_\alpha + f_\beta \Delta H_\beta$ is the weighted heat of fusion of two eutectic phases and C_p is the specific heat of the liquid. Iv is the Ivantsov function, $Iv(u) = u \exp(u) E_1(u)$, in which $E_1(u) = \int_u^\infty \exp(-v)/vdv$ is the first exponential integral function. $P_t = VR/(2\alpha)$ denotes the thermal Peclet number with α the coefficient of thermal diffusion in the liquid.

The melt undercooling ΔT is the sum of ΔT_c and ΔT_t . Combining Equations 12, 14, and 19, we obtain the following.

$$\Delta T = \Delta T_c + \Delta T_r + \Delta T_k + \Delta T_t = m^v \left[\left(Q_0^L \lambda + \frac{1}{\mu} \right) V + \frac{a^L}{\lambda} \right] + \frac{\Delta H}{C_p} Iv(P_t) \quad (20)$$

To analyze the behavior of interlamellar spacing λ , we apply minimum undercooling principle,^{12–14} that is, $\partial \Delta T / \partial \lambda = 0$. Using Equation 20, this leads to the following relationship for the lamellar spacing as a function of velocity¹⁸:

$$\lambda^2 V = a^L / Q^L \quad (21)$$

$$Q^L = \frac{1}{f_\alpha f_\beta} \frac{1-k}{D} \left(P + \lambda \frac{\partial P}{\partial \lambda} \right) \quad (22)$$

From Equations 20 and 21, the relationship of undercooling and interlamellar can be obtained as follows.

$$\Delta T = m^v \frac{a^L}{\lambda} \left[1 + \frac{P}{P + \lambda \frac{\partial P}{\partial \lambda}} + \frac{1}{\mu Q^L \lambda} \right] + \frac{\Delta H}{C_p} Iv(P_t) \quad (23)$$

As a result of solutions 20–23 together with Equations (10) and (11), we can determine the growth velocity V and lamellar spacing λ as functions of the melt undercooling ΔT . Under local equilibrium condition in the diffusion field, $V_D \rightarrow \infty$, the system of Equations 20–23 transforms to the expression $\Delta T - V - \lambda$ previously obtained in LZ (with thermal and kinetic contributions to undercooling) or TMK model (without thermal and kinetic contributions to undercooling).

2.5 | The equation for $V \geq V_D$

For case of $V \geq V_D$, the atoms have no time to diffuse and redistribution at the interface (bulk phases). Interfacial composition, average composition, and initial (nominal) composition will be the same, that is, $C(x,z) = \bar{C}_\alpha = \bar{C}_\infty = C_\infty$ that means the transition to chemically partitionless solidification (Figure 3B). In this diffusionless regime for two cases of phase diagram (Figure 2), see Equations (10) and (11), one obtains $P = 0$ and $P + \lambda(\partial P / \partial \lambda) = 0$. As such, the parameters of eutectic growth (S_α , S_β , and λ) do not exist that leads to the absence of the expressions $m^v(Q_0^L \lambda V + a^L / \lambda)$ in Equation 20. The interface undercooling can be described by two-folds. First, if the expression $m^v(Q_0^L \lambda V + a^L / \lambda)$ is infinitely large, the crystal phase should select the only α or β phase, or the liquid of the eutectic composition will change to glass.²⁴ Second, $m^v(Q_0^L \lambda V + a^L / \lambda)$ is zero that gives the total undercooling Equation 20 as follows:

$$\Delta T = \Delta T_k + \Delta T_t = \frac{m^v V}{\mu} + \frac{\Delta H}{C_p} Iv(P_t) \quad (24)$$

Thus, at the point $V = V_D$, the total undercooling steeply reduces to $\Delta T_k + \Delta T_t$ with the beginning of the (metastable) chemically homogeneous phase formation.

3 | CONCLUSIONS

We have developed diffusion-limited model for lamellar eutectic couple growing into supercooled liquid based on the treatment of TMK and LZ models. This model explains both the eutectic solidification due to diffusion at $V < V_D$ and at $V \geq V_D$ by suppression of eutectic decomposition due to diffusionless (chemically partitionless) solidification. A transition from chemically partitioned to diffusionless growth leading to formation of metastable supersaturated phases of the initial chemical composition has been predicted. It is shown that the interlamellar spacing between eutectic couple growth and diffusionless growth is changed abruptly at $V = V_D$.

ACKNOWLEDGEMENTS

This work was also financially supported by the German Space Center Space Management (No. 50WM1941), the Science and Technology Program of Shaanxi Province (No. 2016KJXX-87), and the Foundation of Shaanxi Provincial Department of Education (No. 18JS050). Open access funding enabled and organized by Projekt DEAL.

CONFLICT OF INTEREST

This work does not have any conflicts of interest.

AUTHOR CONTRIBUTION

Authors contributed equally to the content of the manuscript.

ORCID

Junfeng Xu  <https://orcid.org/0000-0003-4962-9355>

Peter K. Galenko  <https://orcid.org/0000-0003-2941-7742>

REFERENCES

1. Kurz W, Fisher DJ, Trivedi R. Progress in modelling solidification microstructures in metals and alloys: dendrites and cells from 1700 to 2000. *Int Mater Rev*. 2019;64(6):311-354. <https://doi.org/10.1080/09506608.2018.1537090>
2. Li M, Nagashio K, Ishikawa T, Yoda S, Kurabayashi K. Microtexture and macrotexture formation in the containerless solidification of undercooled Ni-18.7 at.% Sn eutectic melts. *Acta Mater*. 2005;53(3):731-741. <https://doi.org/10.1016/j.actamat.2004.10.029>
3. Wang Z, Lin X, Cao Y, Liu F, Huang W. Formation of anomalous eutectic in Ni-Sn alloy by laser cladding. *Opt Laser Technol*. 2018;99: 154-159. <https://doi.org/10.1016/j.optlastec.2017.08.026>
4. Zhang F, Lai C, Zhang J, Zhang Y, Zhou Q, Wang H. Anomalous eutectics in intermediately and highly undercooled Ni-29.8at.%Si eutectic alloy. *J Cryst Growth*. 2018;495:37-45. <https://doi.org/10.1016/j.jcrysgr.2018.05.012>
5. Xu J, Liu F, Zhang D. In situ observation of solidification of undercooled hypoeutectic Ni-Ni₃B alloy melt. *J Mater Res*. 2013;28(14): 1891-1902. <https://doi.org/10.1557/jmr.2013.165>

6. Song C, Wang S, Liu J, Zhai S. Microstructure and mechanical properties of $\text{Al}_2\text{O}_3/\text{Er}_3\text{Al}_5\text{O}_{12}$ binary eutectic ceramic prepared by Bridgman method. *Materials*. 2018;11(4):1–10, 534. <https://doi.org/10.3390/ma11040534>
7. Duwez P, Willens RH, Klement W Jr. Continuous series of metastable solid solutions in silver-copper alloys. *J Appl Phys*. 1960;31: 1136–1137. <https://doi.org/10.1063/1.1735777>
8. Giessen BC, Ray R, Hahn SH. Extensive interstitial solid solutions of metals in metals. *Phys Rev Lett*. 1971;26(9):509–512. <https://doi.org/10.1103/PhysRevLett.26.509>
9. Miroshnichenko IS. Quenching from the liquid state Metallurgia, Moscow, (1982)
10. Jacobson N. Rapid solidification of Ag-Cu and Ag-Pb alloys. *Mater Sci Eng A*. 1991;133:574–576. [https://doi.org/10.1016/0921-5093\(91\)90137-C](https://doi.org/10.1016/0921-5093(91)90137-C)
11. Gusakova OV, Galenko PK, Shepelevich VG, Alexandrov DV, Rettenmayr M. Diffusionless (chemically partitionless) crystallization and subsequent decomposition of supersaturated solid solutions in Sn-Bi eutectic alloy. *Phil Trans R Soc A*. 2019;377(2143):1–15, 20180204. <https://doi.org/10.1098/rsta.2018.0204>
12. Jackson KA, Hunt JD. Lamellar and rod eutectic growth. *TMS of AIME*. 1966;236:1129–1142. <https://doi.org/10.1016/B978-0-08-092523-3.50040-X>
13. Datye V, Langer JS. Stability of thin lamellar eutectic growth. *Phys Rev B*. 1981;24(8):4155–4169. <https://doi.org/10.1103/PhysRevB.24.4155>
14. Trivedi R, Magnin P, Kurz W. Theory of eutectic growth under rapid solidification conditions. *Acta Metall*. 1987;35(4):971–980. [https://doi.org/10.1016/0001-6160\(87\)90176-3](https://doi.org/10.1016/0001-6160(87)90176-3)
15. Kurz W, Trivedi R. Eutectic growth under rapid solidification conditions. *Metall Trans A*. 1991;22(12):3051–3057. <https://doi.org/10.1007/BF02650266>
16. Ludwig A, Leibbrandt S. Generalised ‘Jackson–Hunt’ model for eutectic solidification at low and large Peclet numbers and any binary eutectic phase diagram. *Mater Sci Eng A*. 2004;375–377:540–546. <https://doi.org/10.1016/j.msea.2003.10.108>
17. Zheng L, Zhang H. Revised form of Jackson–Hunt theory: application to directional solidification of MnBi/Bi eutectics. *J Cryst Growth*. 2000;209(1):110–121. [https://doi.org/10.1016/S0022-0248\(99\)00532-1](https://doi.org/10.1016/S0022-0248(99)00532-1)
18. Li JF, Zhou YH. Eutectic growth in bulk undercooled melts. *Acta Mater*. 2005;53(8):2351–2359. <https://doi.org/10.1016/j.actamat.2005.01.042>
19. Wei XX, Lin X, Xu W, et al. Remelting-induced anomalous eutectic formation during solidification of deeply undercooled eutectic alloy melts. *Acta Mater*. 2015;95:44–56. DOI. <https://dx.doi.org/10.1016/j.actamat.2015.05.014>
20. Galenko P, Herlach D. Diffusionless crystal growth in rapidly solidifying eutectic systems. *Phys Rev Lett*. 2006;96(15):1–4, 150602. <https://doi.org/10.1103/PhysRevLett.96.150602>
21. Galenko P, Jou D. Rapid solidification as non-ergodic phenomenon. *Phys Rep*. 2019;818:1–70. <https://doi.org/10.1016/j.physrep.2019.06.002>
22. Thaddeus BM. *Binary Alloy Phase Diagrams*. Second ed. Materials Park Ohio; 1990.
23. Donaghey L, Tiller W. On the diffusion of solute during the eutectoid and eutectic transformations, Part I. *Mater Sci Eng A*. 1968;3(4): 231–239. [https://doi.org/10.1016/0025-5416\(68\)90015-3](https://doi.org/10.1016/0025-5416(68)90015-3)
24. Wang N, Kalay YE, Trivedi R. Eutectic-to-metallic glass transition in the Al-Sm system. *Acta Mater*. 2011;59(17):6604–6619. <https://doi.org/10.1016/j.actamat.2011.07.015>

How to cite this article: Xu J, Galenko PK. Effects of local nonequilibrium in rapid eutectic solidification—Part 1: Statement of the problem and general solution. *Math Meth Appl Sci*. 2020;1–10. <https://doi.org/10.1002/mma.6960>